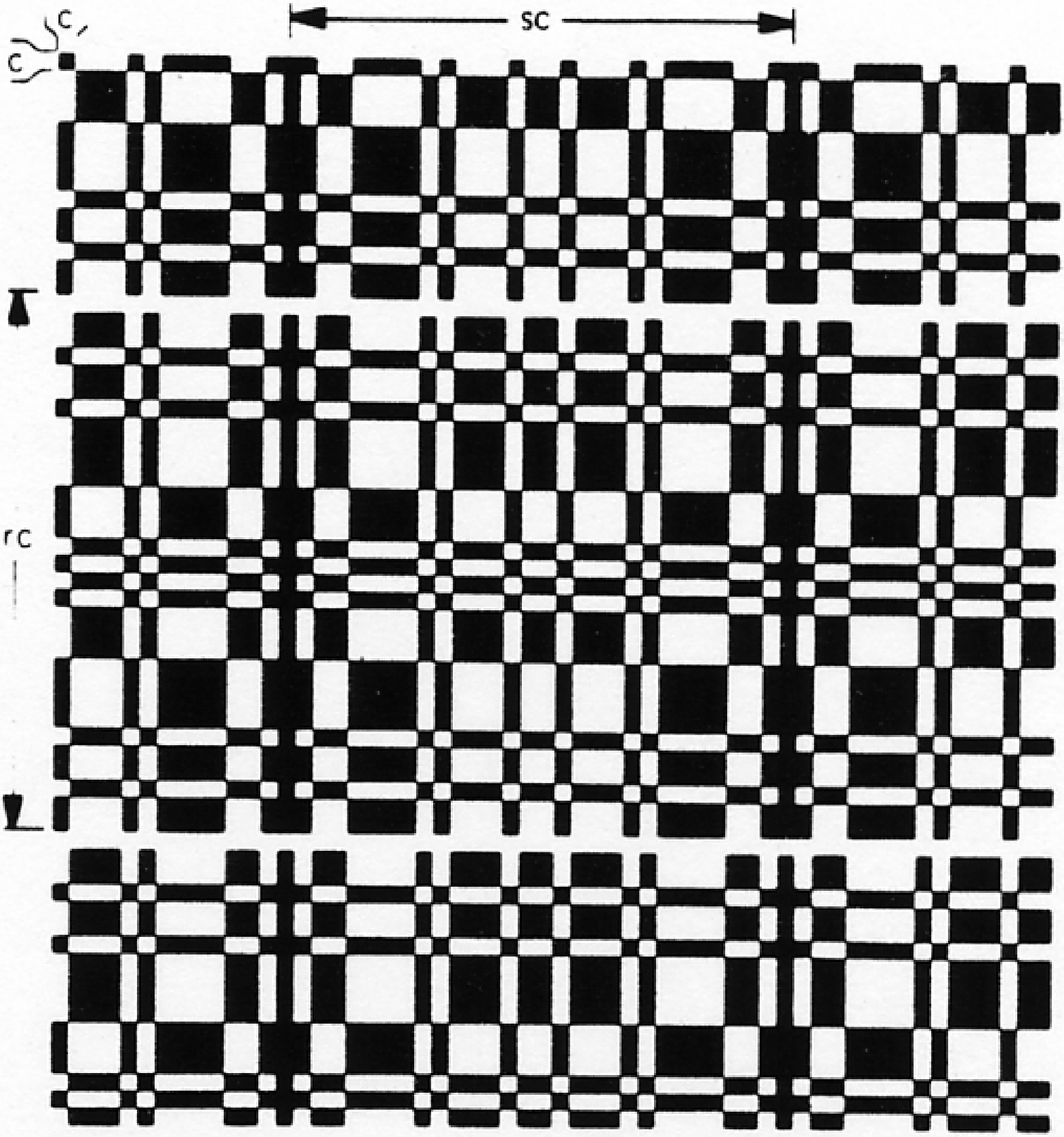

Fig. 1. Two cycles of an $r \times s$ URA pattern. Note it has periods rc and sc with square $c \times c$ pinholes.

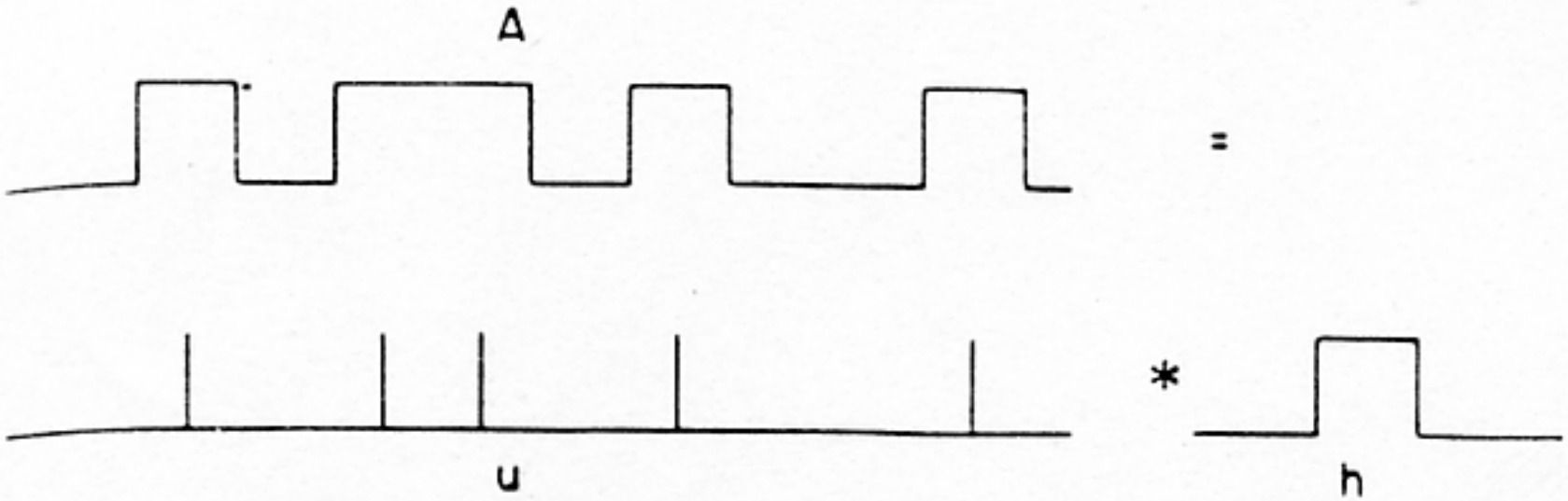

Fig. 2. Demonstration of how the aperture function can be decomposed into a function describing the locations of the pinholes and a function representing the pinhole shape.

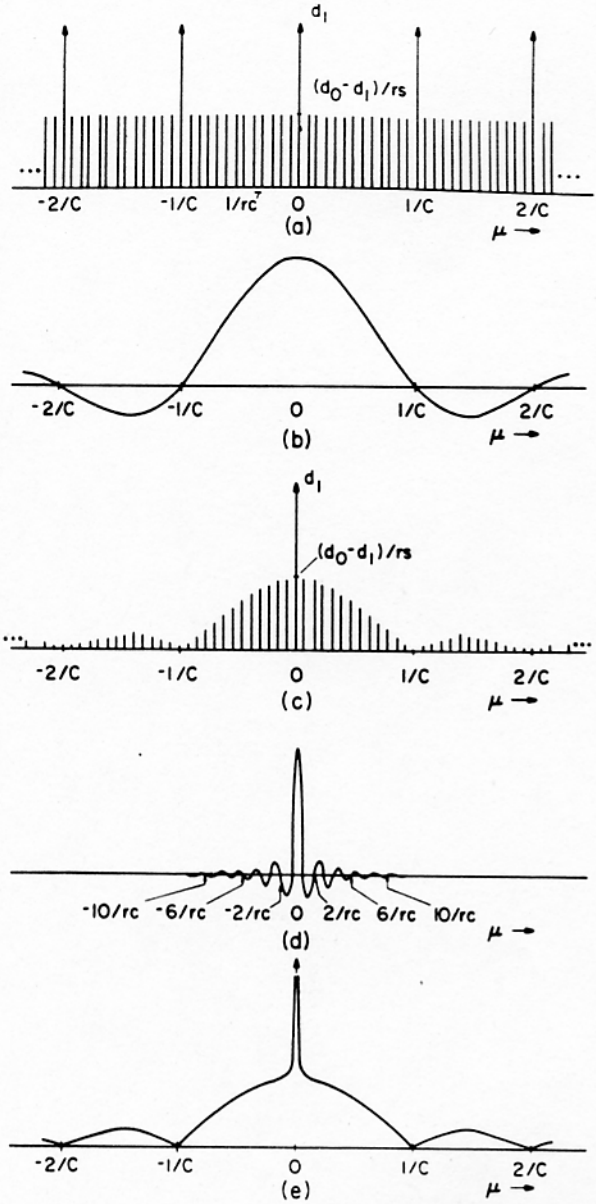

Fig. 3. Various functions used to derive the MTF of a URA aperture: (a) $|U(\mu,\nu)|$; (b) $H(\mu,\nu)$; (c) $|U(\mu,\nu)\cdot H(\mu,\nu)|$; (d) $B(\mu,\nu)$; (e) $|F(A)|$.

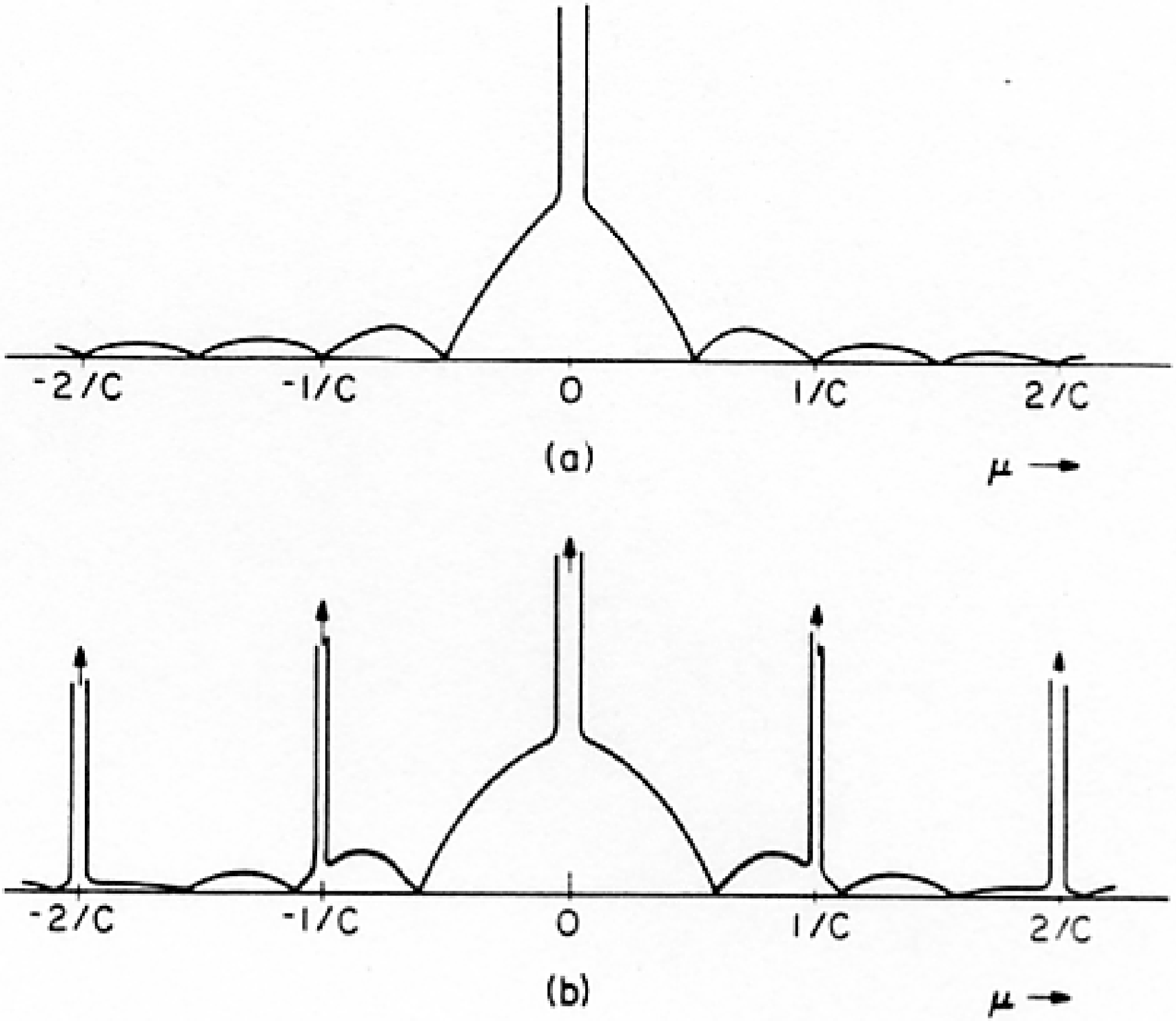

Fig. 4. (a) MTF of a URA whose pinholes are $c/2 \times c/2$ squares; (b) MTF of a URA whose pinholes are round with a diameter of $c/2$.

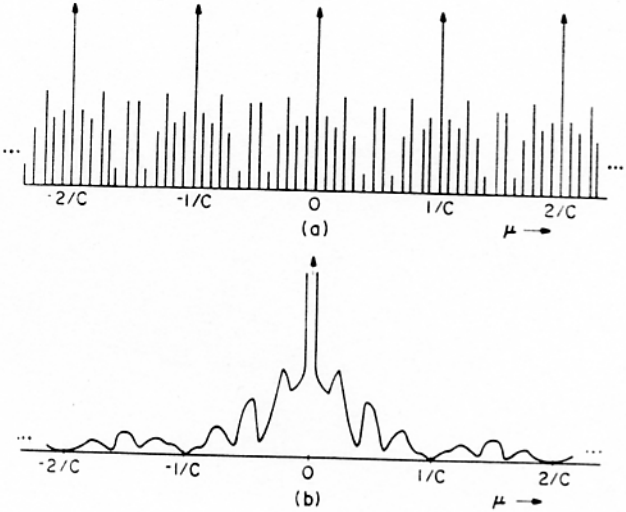

Fig. 5. (a) Fourier transform of $u(x,y)$ for a random array; (b) MTF of a random array.

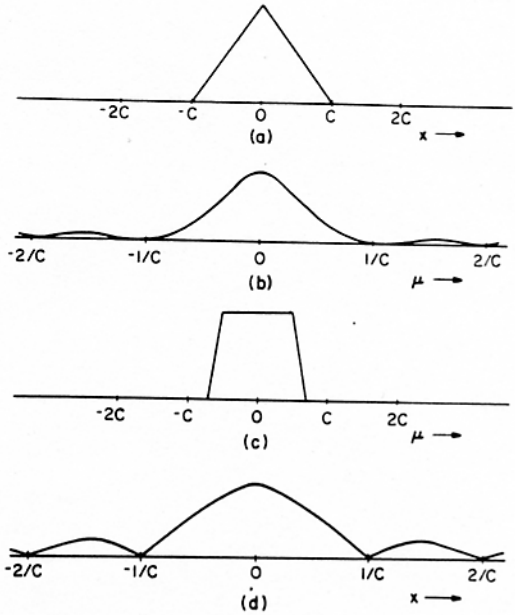

Fig. 6. (a) SPSF for a correlation analysis; (b) MTF for balanced correlation; (c) SPSF for δ decoding; (d) MTF for δ decoding.

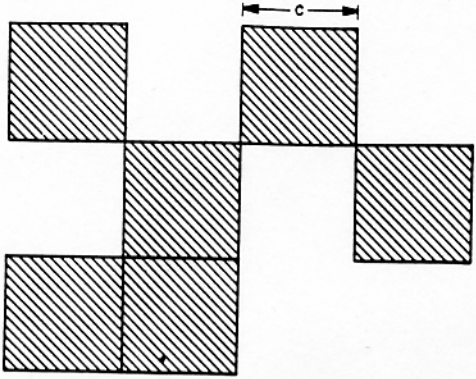

(a)

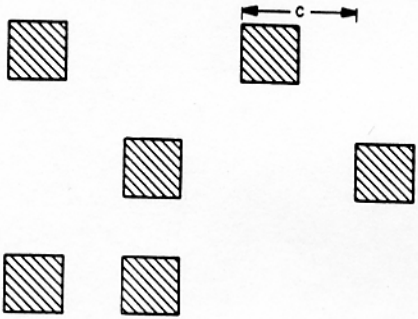

(b)

Fig. 1. (a) A small section of a URA pattern; (b) a small section of a no-two-holes-touching URA pattern.

(same URA function)

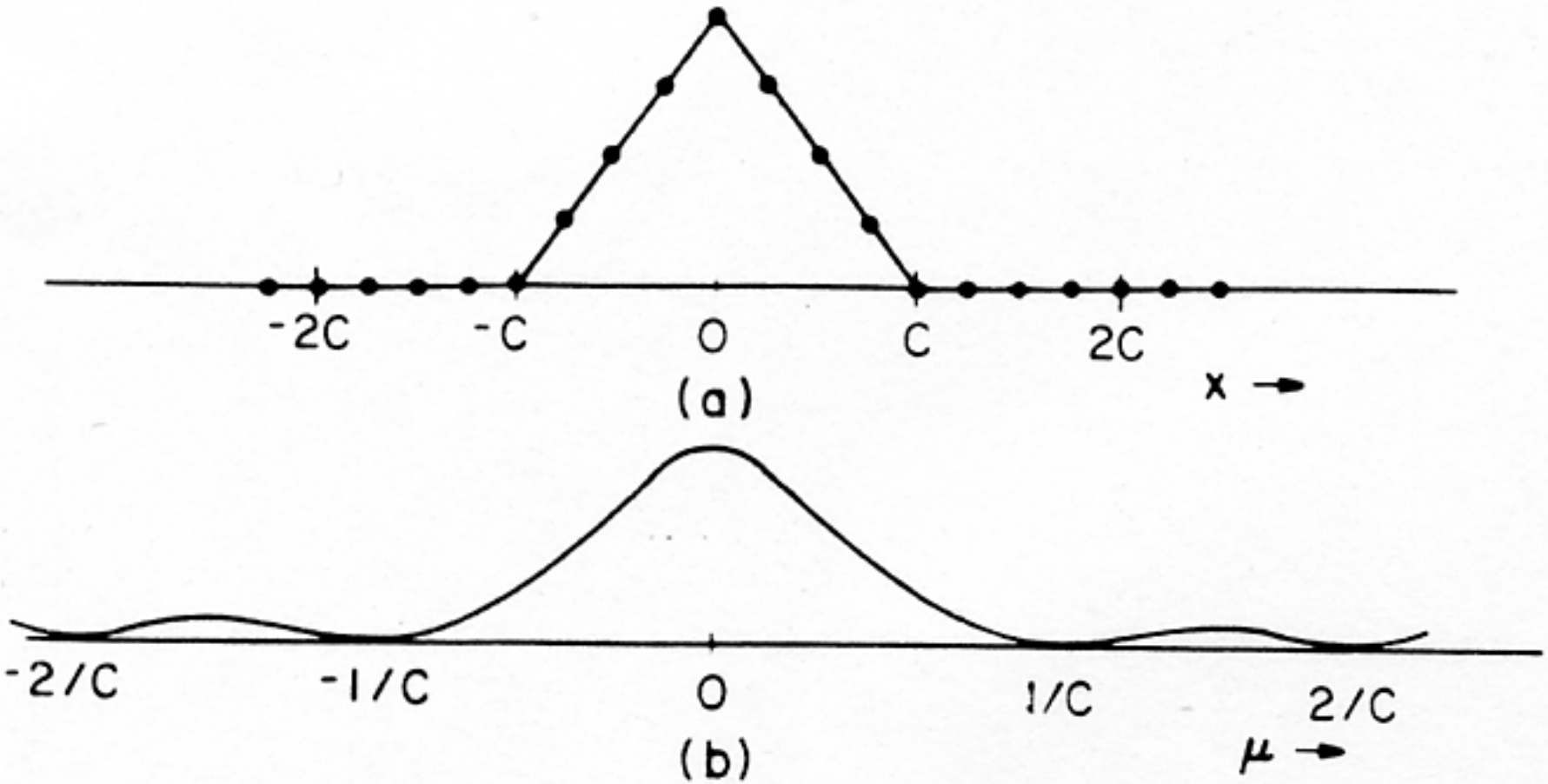

Fig. 5. (a) SPSF and (b) MTF for finely sampled balanced correlation.

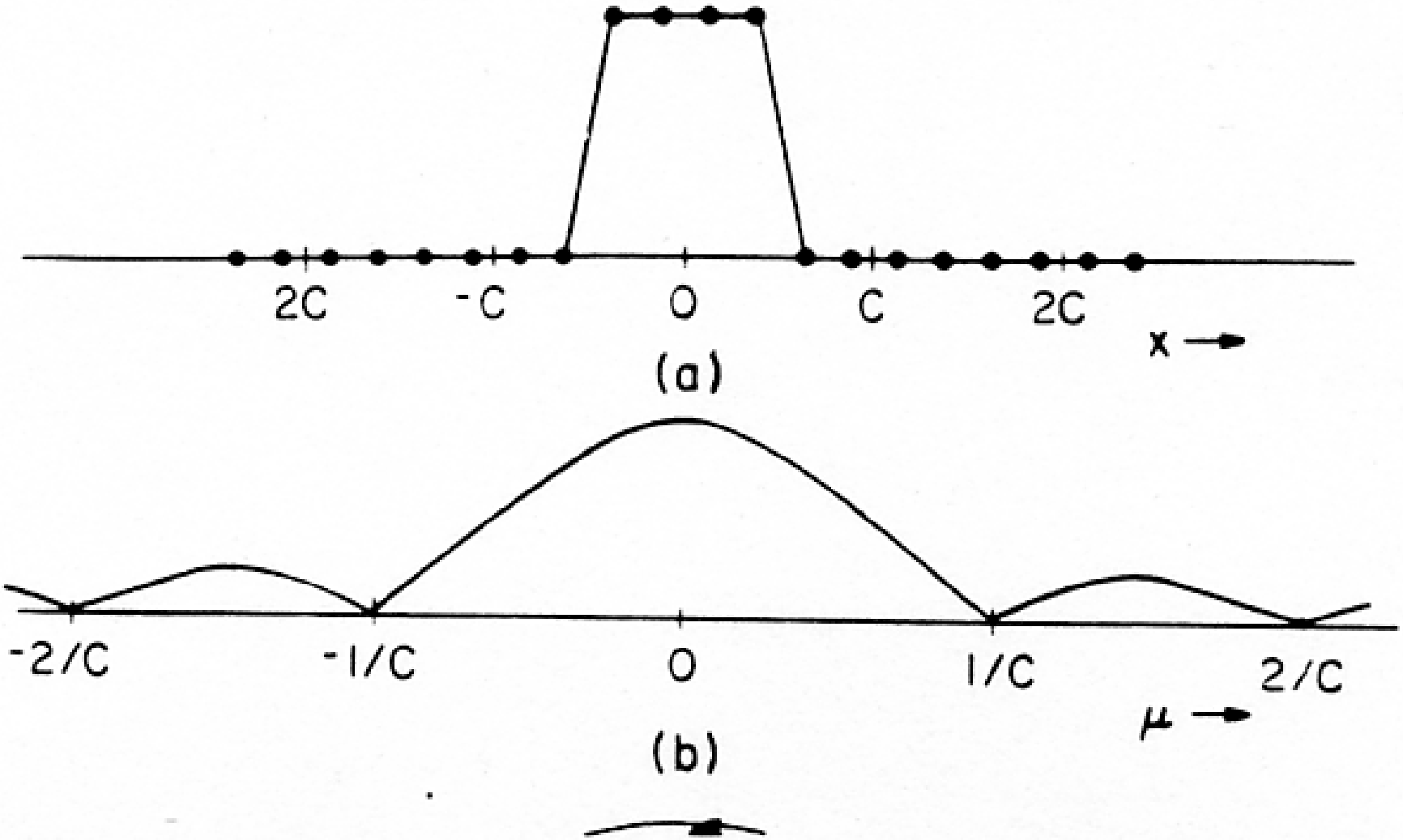

Fig. 8. (a) SPSF and (b) MTF for δ decoding.

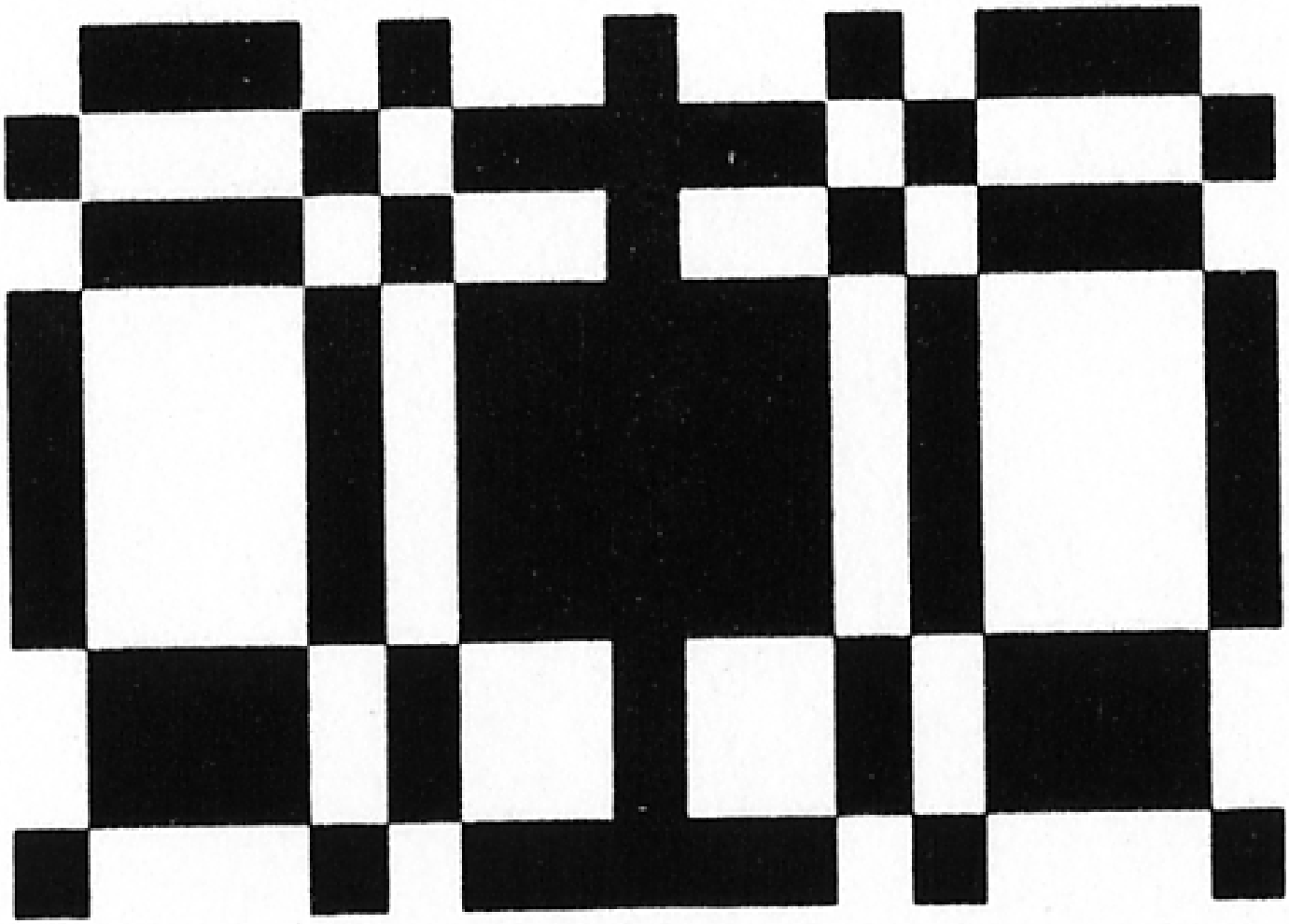

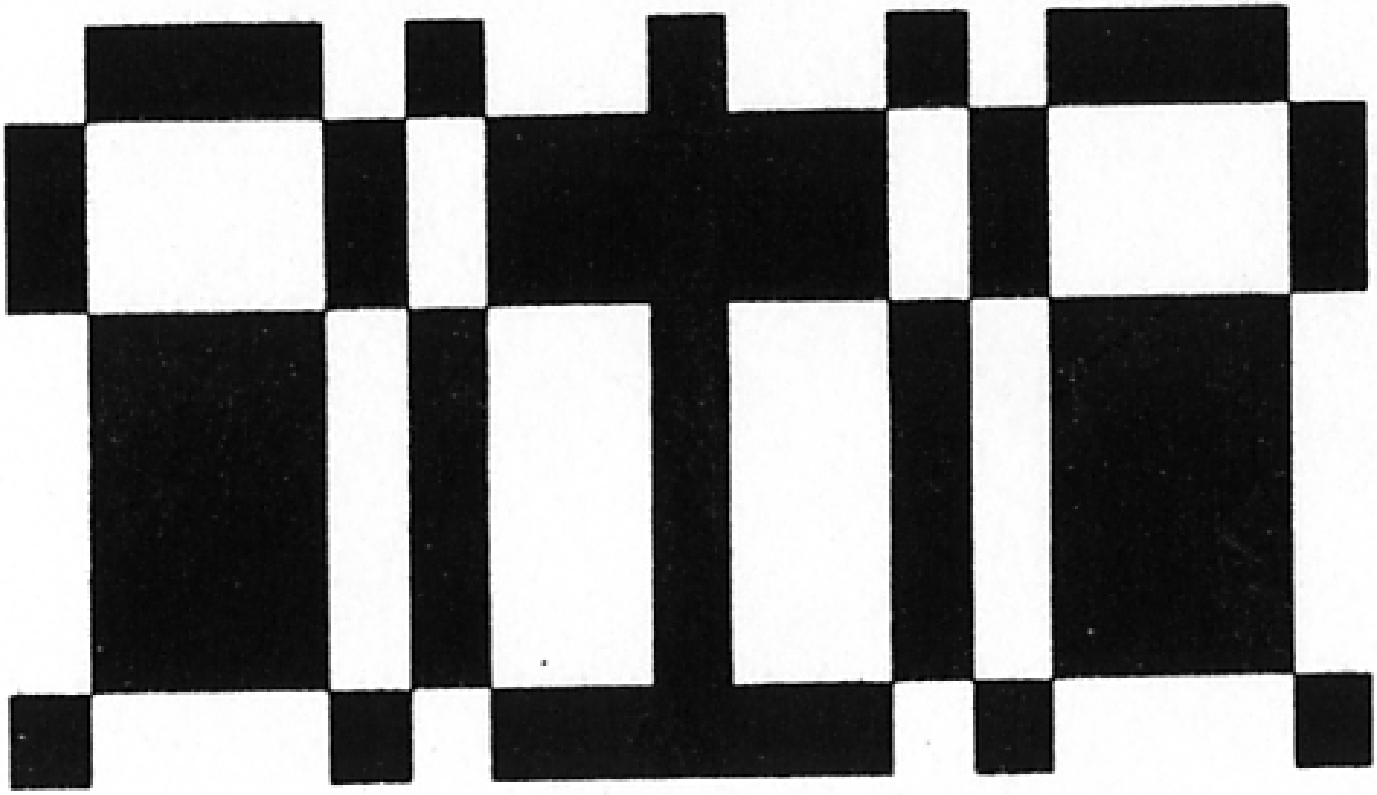

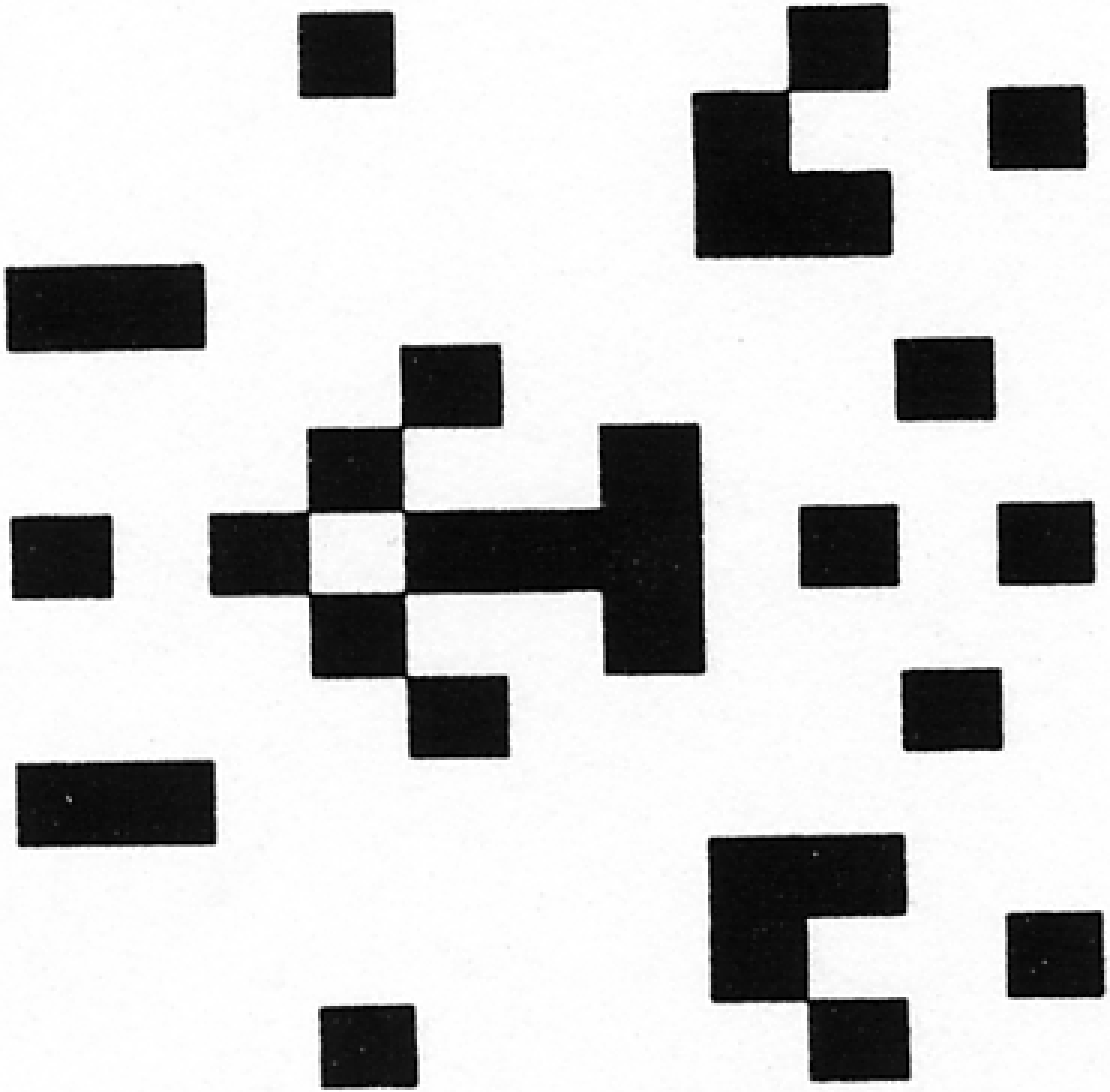

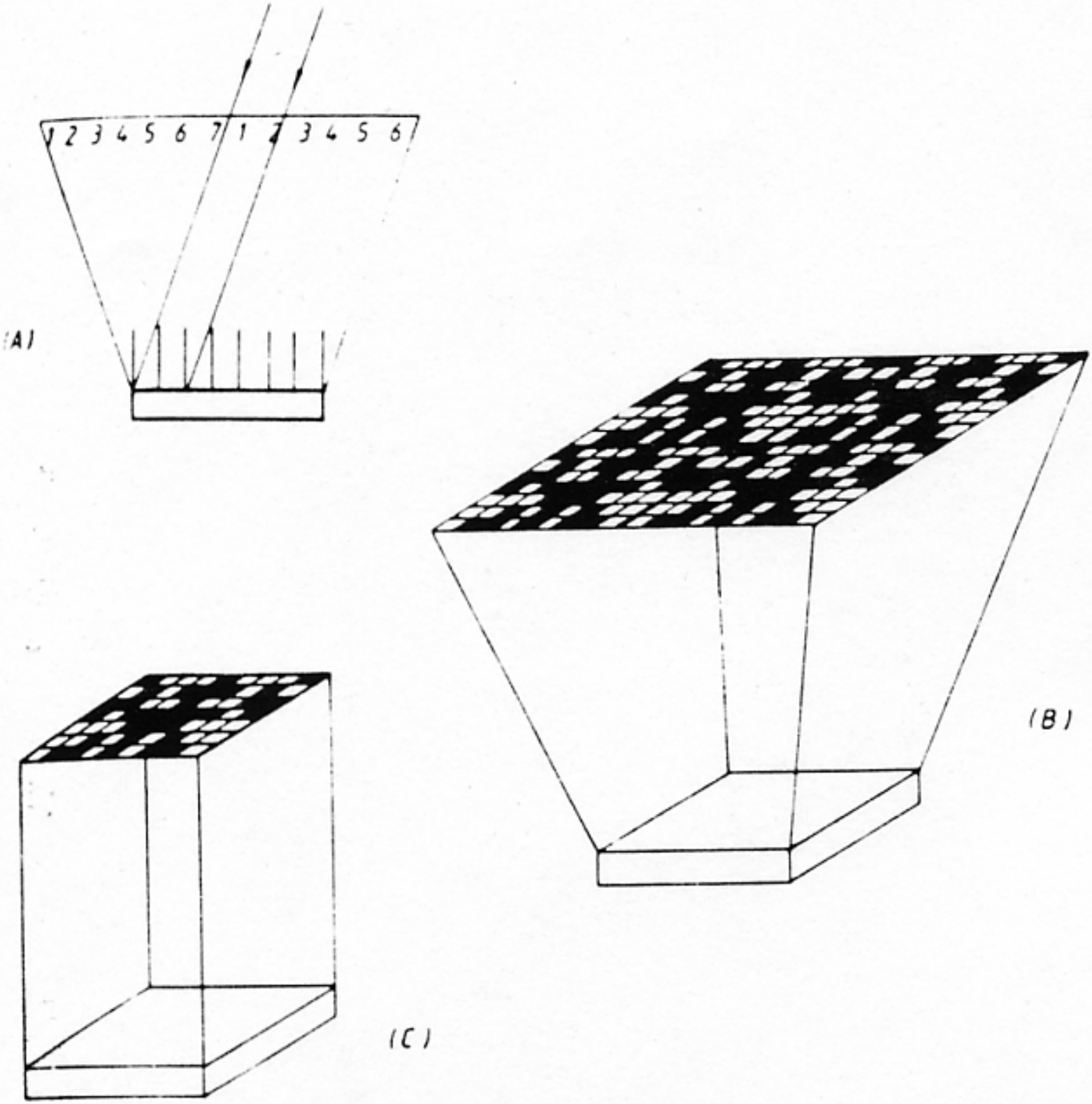

Fig. 2. (a) 1-dimensional cyclic mask coded aperture system, showing use of a slat collimator. (b) 2-dimensional version of (a). (c) Simple, non-cyclic system.

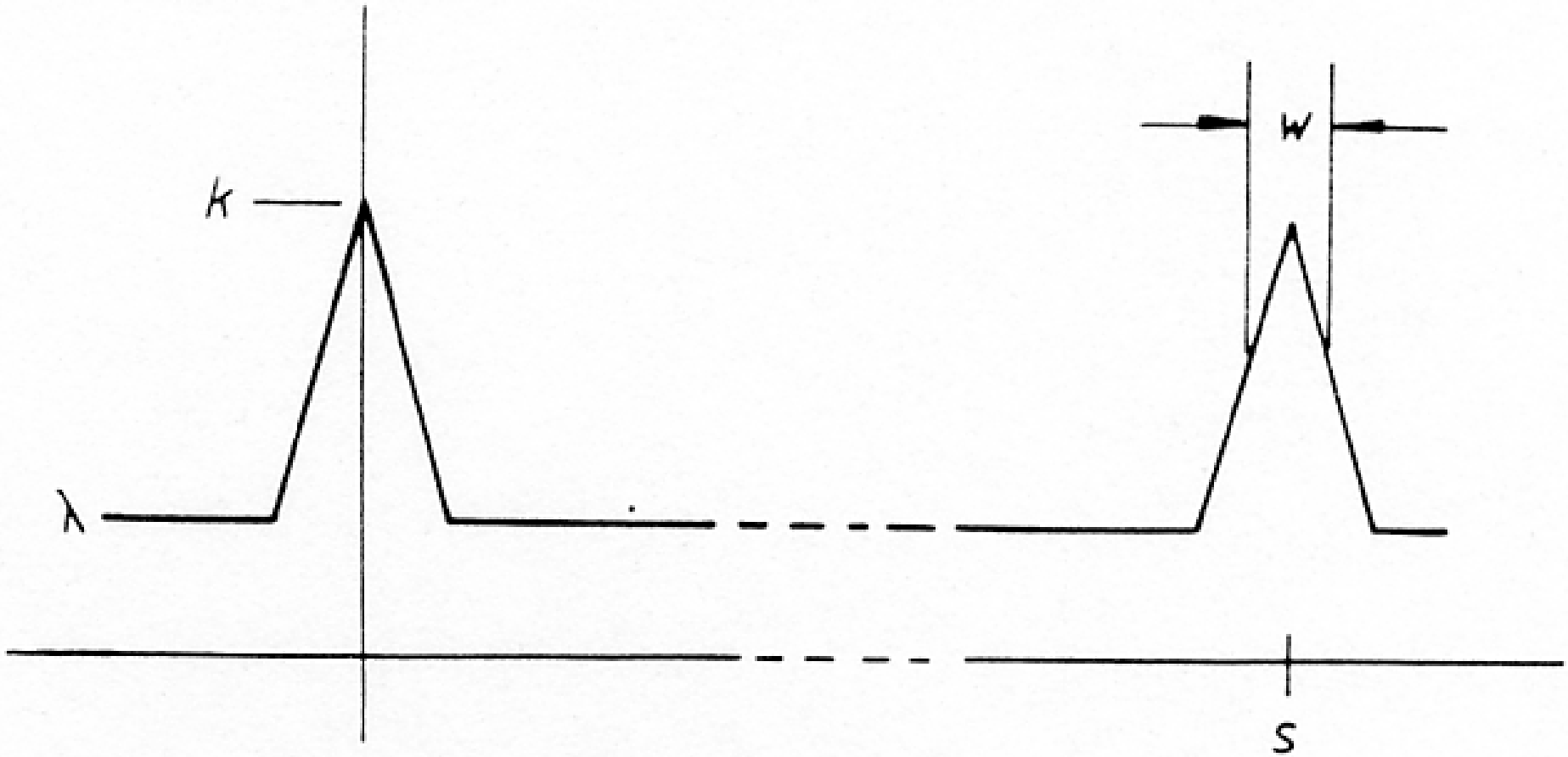

Fig. 3. Autocorrelation function for an n-element mask based on an (n, k, λ) cyclic difference set. The open fraction, f, of such a mask is $f = k/n$ so the peak and dc levels are nf and $-nf^2$.